Bridging Experiment and Computation: In Silico Admet, Protox-III, and Target-Guided Docking of Nitro-Substituted Dichlorodiazadienes

Gulnar Atakishiyeva[1], Nigar Ahmedova [1], Sevinc Mukhtarova [2], Ayten Niyazova [3], Namiq Shikhaliyev[4*], Abel Maharramov [1]

[1]Baku State University, 23 Academician Zahid Khalilov Street, Baku 1148 , Azerbaijan, atakishiyeva.gulnar.91@gmail.com
[2]Azerbaijan Technical University, 25 Huseyn Javid Avenue, Baku 1073, Azerbaijan sevinc.muxtarova@aztu.edu.az,
[3]Azerbaijan State University of Economics (UNEC), 6 Istiglaliyyat, Baku, Azerbaijan, niyazova.ayten@yandex.ru
[4]Baku Engineering University, Khirdalan city, 120 AZ0101 Hasan Aliyev street, Baku, Azerbaijan, namiqst@gmail.com

Abstract. This study integrates experimental findings with computational analysis to elucidate the pharmacokinetic, toxicological, and molecular interaction profiles of six nitro-substituted dichlorodiazadiene derivatives. Comprehensive ADMET modeling using ADMET-AI and vNN-ADMET revealed high oral absorption (HIA ≈ 1.0) and strong plasma protein binding, accompanied by moderate CYP1A2 and CYP2C19 inhibition and acceptable excretion kinetics. ProTox-III predictions classified the compounds within GHS toxicity classes 3–4 (LD_{50} = 90–710 mg/kg), highlighting mutagenicity, carcinogenicity, and cardiotoxicity as key structural liabilities linked to nitro- and azo-functionalities. Among the evaluated molecules, Compounds 1 and 2 exhibited comparatively safer profiles, whereas Compounds 3 and 4 showed acute toxicity and genotoxic potential. Molecular docking simulations performed with SwissDock (AutoDock Vina engine) identified FabH (4IJ0) as the preferential binding target of Compound 4 (ΔG = −4.987 kcal/mol) compared with GyrB (2XCT) (ΔG = −3.850 kcal/mol). The binding network involved hydrogen bonding, π–π stacking, and halogen interactions that rationalize the experimentally observed antibacterial potency. Overall, the integrated ADMET–toxicity–docking workflow underscores FabH inhibition as a plausible mechanism of action and provides a predictive framework for structure-guided optimization of safer, more selective dichlorodiazadiene analogues.

Keywords: dichlorodiazadiene, ADMET-AI, ProTox-III, molecular docking

R. Rzayev et al. (eds.), *Proceedings of the International Conference on Current Problems in Engineering and Applied Sciences (ICCPEAS 2025)*, Advances in Engineering Research 299,
https://doi.org/10.2991/978-94-6239-668-5_8

1. Introduction

In recent years, diazadiene and diazabutadiene derivatives obtained through the interaction of hydrazones with halogenating reagents have become the focus of considerable attention in organic synthesis and materials chemistry. The reaction of phenylhydrazones with CCl_4 or CBr_4 in the presence of a CuCl catalyst yields 1,1-dichloro- and 1,1-dibromodiazadienes, which have been evaluated both as novel types of azo dyes and as promising bioactive molecules [1–5]. The electron-accepting nature of the nitro group promotes the formation of intra- and intermolecular pnictogen (N···Cl, N···Br) and halogen (Cl···O, Br···O) interactions, thereby enhancing crystal stability and molecular self-organization. Such noncovalent interactions play a crucial role not only in crystal engineering but also in pharmacophore modeling, and the structural–functional investigation of nitro-substituted dichlorodiazadienes provides a valuable foundation for the rational design of target-oriented compounds.

Studies conducted between 2018 and 2022 demonstrated that the expansion of the π-conjugation system and the presence of electron-accepting substituents significantly influence the spectral, crystalline, and biophysical properties of these molecules, improving their stability through noncovalent contacts such as N···Cl, O···H, and π···π stacking interactions [6–8]. At the same time, the bioactivity potential of these systems is being assessed using *in silico* approaches, particularly ADMET and toxicity analyses. Platforms such as SwissADME, ProTox-III, vNN-ADMET, and ADMET-AI are recognized as effective tools for early-stage pharmacokinetic prediction [9–12]. The "bPK-score" model proposed by Beckers *et al.* integrates nearly one hundred parameters to quantify molecular developability [13], while Venkatraman *et al.* improved prediction reliability through the fingerprint-based FP-ADMET approach [14]. Bissenbay *et al.* demonstrated the efficiency of SwissADME and ProTox-III in evaluating the bioavailability and toxicity profiles of piperidine derivatives [15]. Furthermore, artificial intelligence and deep learning algorithms have substantially improved prediction accuracy in the field of computational toxicology [16]. Consequently, *in silico* assessment of nitro- and halogen-substituted dichlorodiazadienes obtained via olefination reactions allows for a deeper understanding of their chemical reactivity and pharmacological potential.

Recent investigations have highlighted β-ketoacyl-acyl carrier protein synthase III (FabH), which catalyzes the initiation of fatty acid biosynthesis, and DNA gyrase B (GyrB), responsible for DNA supercoiling, as major enzymatic targets in antibacterial drug design [17–19]. The catalytic site of FabH, comprising Cys112, His244, and Asn274 residues, has been identified as a promising target for selective inhibitor development [20–22]. The study by Dhawale *et al.* (2022) confirmed that natural polyphenol and triazine derivatives exhibited strong FabH binding affinities (−8.6 kcal/mol) and favorable ADMET profiles [23]. In contrast, studies on GyrB inhibitors—including coumarin, indazole, and triazine derivatives—employed 3D-QSAR and molecular dynamics analyses to define steric and electrostatic fields essential for designing more selective inhibitors; CoMFA and CoMSIA models (R^2_pred = 0.68–0.77) identified key amino acid residues such as Ile54, Glu55, Arg83, Val86, and Thr128 [17,18]. Additionally, *in silico* modeling of curcumin analogues against *Salmonella typhi* β-lactamase and L,D-transpeptidase enzymes revealed binding energies up to −8.15 kcal/mol and satisfactory ADMET characteristics, confirming the antimicrobial potential of natural phenolic systems [24]. Thus, *in silico* analysis of synthetic and naturally derived hydrazone and diazadiene derivatives targeting both FabH and GyrB enzymes suggests a synergistic antibacterial mechanism through the simultaneous inhibition of fatty acid biosynthesis and DNA supercoiling pathways

Therefore, the present study aims to integrate experimental and computational data to predict the ADMET behavior, toxicity profiles, and target-specific binding mechanisms of nitro-substituted dichlorodiazadiene derivatives.

2. Materials and Methods

2.1. Ligand Preparation

Six dichlorodiazadiene derivatives were selected for in silico evaluation. The compounds were designed by varying methyl substitution patterns across the phenyl rings, while retaining the core dichlorodiazadiene scaffold. The optimized molecular structures were generated from their SMILES notations using the ChemDraw and Avogadro software, followed by geometry optimization under MMFF94 force field conditions.

The SMILES representations of the compounds are as follows:

1. **Compound 1:**
CC1=CC=C(C=C1)\N=N\C(=C(Cl)Cl)C1=C(C=CC=C1)N(=O)=O
2. **Compound 2:**
CC1=CC(=CC(C)=C1)\N=N\C(=C(Cl)Cl)C1=C(C=CC=C1)N(=O)=O
3. **Compound 3:**
CC1=CC=C(C=C1)\N=N\C(=C(Cl)Cl)C1=CC(=CC=C1)N(=O)=O
4. **Compound 4:**
CC1=CC(=CC(C)=C1)\N=N\C(=C(Cl)Cl)C1=CC(=CC=C1)N(=O)=O
5. **Compound 5:**
CC1=CC=C(C=C1)\N=N\C(=C(Cl)Cl)C1=CC=C(C=C1)N(=O)=O
6. **Compound 6:**
CC1=CC(=CC(C)=C1)\N=N\C(=C(Cl)Cl)C1=CC=C(C=C1)N(=O)=O

All ligands were converted into three-dimensional (3D) structures and energy-minimized prior to further analysis.

Note: The detailed synthetic route and spectral data can be found in [1].

2.2. ADMET and Toxicological Prediction Platforms

ADMET-AI [25]

The ADMET-AI webserver (https://admet.ai/) was used to predict Absorption, Distribution, Metabolism, Excretion, and Toxicity (ADMET) parameters.

ADMET-AI employs ensemble machine learning models trained on large-scale pharmacokinetic datasets and provides high-throughput screening of molecular properties. The following endpoints were analyzed:

- Physicochemical parameters (Molecular Weight, LogP, TPSA, HBA/HBD);
- Absorption-related indices (Human Intestinal Absorption, Oral Bioavailability, Solubility, PAMPA);
- Distribution descriptors (Plasma Protein Binding, Volume of Distribution, BBB permeability);
- Metabolic interactions (CYP1A2, CYP2C19, CYP2D6, CYP3A4 inhibition);
- Excretion (t½, Clearance);
- Toxicity endpoints (hERG block, Ames mutagenicity, DILI, Carcinogenicity).

Each compound's property dataset was extracted from ADMET-AI output panels (Fig. S5).

ProTox-III [26]

The ProTox-III server (https://tox-new.charite.de/protox_III/) was utilized to assess acute oral toxicity (LD_{50}), GHS toxicity classification, organ-level toxicities, and molecular initiating events (MIEs).

ProTox-III integrates machine learning with structural similarity and pharmacophore alignment to predict toxicity endpoints. The following predictions were collected:

- Acute oral LD_{50} and toxicity class (1–6 scale);
- Organ-specific toxicities (hepatotoxicity, nephrotoxicity, neurotoxicity, immunotoxicity);
- Tox21 nuclear receptor and stress pathway activation;
- Mitochondrial membrane potential (MMP) and transthyretin (TTR) interactions;
- Cytochrome P450 inhibition (CYP1A2, 2C19, 2C9, 2D6, 3A4, 2E1).

An example of ProTox-III output for Compound 1 (LD_{50} = 710 mg/kg, Class 4) is shown in Fig. S1-3**.**

vNN-ADMET [27]

The vNN-ADMET platform (https://vnnadmet.bhsai.org/) was applied to validate and cross-check ADMET-AI and ProTox-III results.

This system uses validated nearest-neighbor neural networks (vNNs) to predict toxicity endpoints within defined applicability domains. The following models were applied:

- hERG Blocker;
- Mitochondrial Membrane Potential (MMP) Disruption;
- Ames Mutagenicity;
- DILI and Cytotoxicity;
- CYP Inhibition (1A2, 2C9, 2C19, 2D6, 3A4);
- P-glycoprotein (P-gp) Inhibition/Substrate status;
- Maximum Recommended Therapeutic Dose (MRTD).

All molecules fell partially outside the applicability domain for DILI and CYP inhibition, and these endpoints were therefore treated as low-confidence predictions. Representative vNN-ADMET interface snapshots are shown in Fig. S4.

2.3. Data Visualization

The obtained toxicity and pharmacokinetic parameters were visualized using Python (matplotlib, seaborn) [28, 29].

- Scatter plots (Fig. 2) summarized correlations between molecular weight and dose.
- Radar charts (Fig. 5, and 4) depicted integrated ADMET and toxicity profiles.
- Heatmaps (Fig. 1) illustrated organ-level and receptor-based "Active/Inactive" distributions.
- Biological target interactions are presented as a comparative bar chart (Fig. 3).

2.4. Compound Selection and Background

The present molecular docking study was designed based on previously reported *dichlorodiazadiene* derivatives synthesized and characterized by Shikhaliyev *[1]*.

In that study, twelve nitro- and methyl-substituted dichlorodiazadienes were prepared, and their antibacterial activities were screened against *Escherichia coli*, *Acinetobacter baumannii*, *Klebsiella pneumoniae*, *Pseudomonas aeruginosa*, and *Staphylococcus aureus*. Among them, Compound 4 exhibited the highest antibacterial activity, showing the lowest MIC values (31.25 μg/mL against *A. baumannii* and *S. aureus*).

To elucidate the molecular basis of this experimental observation, only Compound 4—which demonstrated the strongest inhibitory effect—was selected for *in silico* evaluation. Docking simulations were carried out against two biologically relevant bacterial targets: FabH (β-ketoacyl-ACP synthase III, PDB ID: 4IJ0) and GyrB (DNA gyrase subunit B, PDB ID: 2XCT). This dual-protein approach allowed for comparative insight into the compound's possible binding mechanisms.

Ligand and protein preparation [30, 31]

The 3D structure of Compound 11 was constructed from its SMILES notation using the RDKit toolkit and energy-minimized with the MMFF94 force field. The structure was saved in PDB format and uploaded to the SwissDock web server (2024 version), which operates on the AutoDock Vina scoring function.

Protein structures for FabH (4IJ0) and GyrB (2XCT) were retrieved from the Protein Data Bank (https://www.rcsb.org/). All water molecules, ligands, and cofactors were removed; hydrogen atoms were added, and missing side chains were rebuilt using SwissDock's automatic preprocessing algorithm. Each receptor file was saved as 4ij0_modified.pdb and 2xct_modified.pdb, respectively.

2.5. Docking Protocol

Docking simulations were performed under the Accurate Mode with default parameters. The grid box dimensions were automatically defined around the detected binding cavities of the receptors. For each protein–ligand pair, 20 distinct binding conformations (poses) were generated.

The scoring results were evaluated based on the predicted binding free energies (ΔG, kcal/mol), with lower values indicating stronger interactions. The top-ranked conformations were selected for post-docking visualization.

2.6. Visualization and Interaction Analysis [32]

The best docking poses were imported into UCSF ChimeraX for interaction mapping and visualization. Non-covalent interactions—hydrogen bonds, van der Waals forces, halogen interactions, and π–π stacking—were identified using the "contacts" and "hbonds" tools with a 4.0 Å cutoff.

The receptor surface was generated to represent the spatial fitting of the ligand within the binding pocket, and hydrogen bonds were displayed as yellow dashed lines.

Summary of computational setup

Parameter	FabH (4IJ0)	GyrB (2XCT)
Docking software	SwissDock (AutoDock Vina-based)	SwissDock (AutoDock Vina-based)
Grid definition	Automatic (SwissDock cavity)	Automatic (SwissDock cavity)
Binding modes generated	***20***	***20***
Lowest binding energy (kcal/mol)	*-4987*	*-3850*
Visualization tool	UCSF ChimeraX 1.8	UCSF ChimeraX 1.8

3. Results and Discussion

Computational ADMET and toxicity prediction tools (ADMET-AI, vNN-ADMET, and ProTox-III) were employed to provide a multi-tier in-silico assessment of pharmacokinetic behavior and safety liabilities, combining machine-learning-based absorption and metabolism modeling (ADMET-AI), neural-network toxicity validation within applicability domains (vNN-ADMET), and mechanistic endpoint classification covering organ- and receptor-level toxicities (ProTox-III).

Overview of Toxicological Evaluation (ProTox-III)

ProTox-III analysis provided comprehensive predictions for acute toxicity (LD_{50}), GHS toxicity class, organ-specific toxicities, Tox21 nuclear receptor and stress pathway activations, molecular initiating events (MIEs), and cytochrome P450 (CYP) metabolic interactions across the six dichlorodiazadiene derivatives.

The results indicate that the series can be divided into two toxicity clusters based on acute toxicity:

- Compounds 3 and 4 belong to Class 3 ($LD_{50} \approx 90$ mg/kg), representing the most toxic members of the series.
- Compounds 1, 2, 5, and 6 fall into Class 4 ($LD_{50} \approx 476–710$ mg/kg), showing moderate acute toxicity.

This distinction highlights that, despite structural similarities, the compounds differ significantly in tolerability under acute exposure conditions.

Genotoxicity and Carcinogenicity

Mutagenicity signals were consistently "Active" across the series, with the highest probabilities observed for Compounds 3–6 (≈ 0.79–0.82). Carcinogenicity was moderately positive for all compounds (≈ 0.57–0.58). These findings suggest that nitro and azo motifs within the molecular framework may contribute to the formation of electrophilic intermediates, consistent with known mutagenic mechanisms.

Cardiotoxicity and CNS Penetration

All compounds displayed moderate cardiotoxicity signals (≈ 0.56–0.63), aligning with potential off-target effects on cardiac repolarization (hERG-independent models).

Blood–brain barrier (BBB) permeability was predicted as "Active" for all compounds (≈ 0.75–0.77), indicating possible central nervous system exposure risks. Combined with the lipophilic aromatic character of these molecules, this could increase the likelihood of CNS-related adverse *effects.*

Organ-level and Systemic Toxicities

Other organ-specific endpoints—including hepatotoxicity, nephrotoxicity, and neurotoxicity—were generally "Inactive" (≈ 0.50–0.80), suggesting low direct toxicity in these tissues. Immunotoxicity remained consistently "Inactive" (≈ 0.98–0.99), indicating a low probability of immune suppression or hypersensitivity reactions.

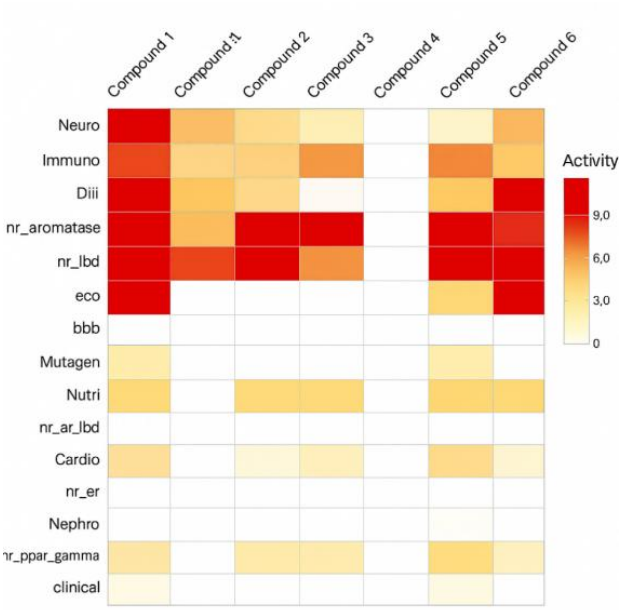

Fig. 1 Organ- and receptor-level active/inactive toxicity endpoints for six dichloro-diazadiene derivatives (ProTox-III heatmap).

Molecular Initiating Events (MIEs)

Mechanistic endpoints highlighted several recurring "Active" responses:

- ❖ Mitochondrial membrane potential (MMP) disruption (≈ 0.51–0.57),
- ❖ Transthyretin (TTR) interaction (≈ 0.50–0.59),
- ❖ and occasional THRβ activation (~ 0.50).

These may collectively indicate the potential for mitochondrial stress and endocrine interference, both consistent with the observed toxicity profiles.

CYP Metabolic Interaction Profile

The CYP profiling revealed a series-wide "Active" signal for CYP2C9 (≈ 0.66–0.68), suggesting possible inhibitory or competitive interactions leading to drug–drug interaction (DDI) risks. Occasional CYP2C19 borderline activity was noted for Compounds 3 and 5 (~ 0.50). Other major isoforms (CYP1A2, 2D6, 3A4, 2E1) remained inactive, reflecting a relatively selective metabolic liability.

Comparative and Mechanistic Interpretation

Fig. 1 illustrates the distribution of LD_{50} values and toxicity classes for all compounds. The clear separation between Classes 3 and 4 supports a structure–toxicity relationship where minor functional modifications (especially nitro/azo presence) strongly affect acute toxicity outcomes.

Fig. 2 visualizes the organ- and receptor-level active/inactive endpoints, highlighting a distinct clustering between active (red) and inactive (green) toxicity networks. Compounds 3–4 cluster in the active region, correlating with their high acute toxicity

and mutagenic profiles, whereas Compounds 1–2 are positioned in the inactive domain, reflecting their comparatively safer behavior.

Fig. 3 compares the molecular weight and dose value distributions, demonstrating that compounds with similar molecular weights (320–380 g/mol) can still show highly divergent dose requirements (476–2300 mg/kg). This reinforces that molecular weight alone is not predictive of toxicity**.**

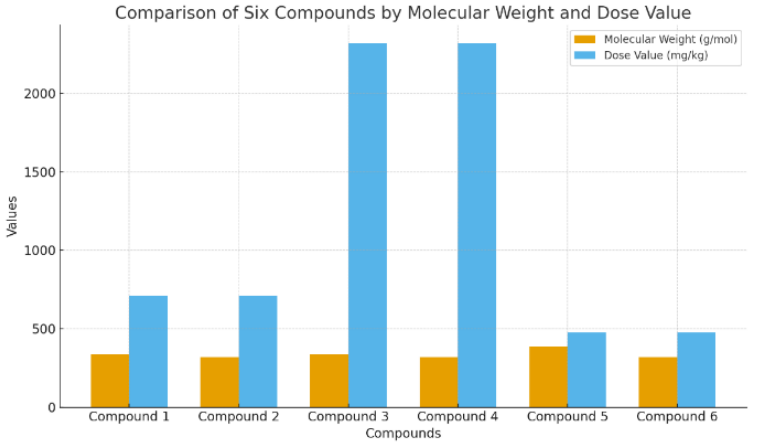

Fig. 2. Distribution of LD_{50} values and GHS toxicity classes for dichlorodiazadiene derivatives predicted by ProTox-III.

Recommendations and Design Implications

Mechanistic correlations suggest that:

- ❖ Nitro and azo groups may drive mutagenicity via nitrenium/azo radical intermediates during bioreduction.
- ❖ MMP activation implies mitochondrial dysfunction potential, while TTR binding indicates possible thyroid hormone transport interference.
- ❖ BBB activity combined with lipophilicity raises CNS exposure and off-target concerns.

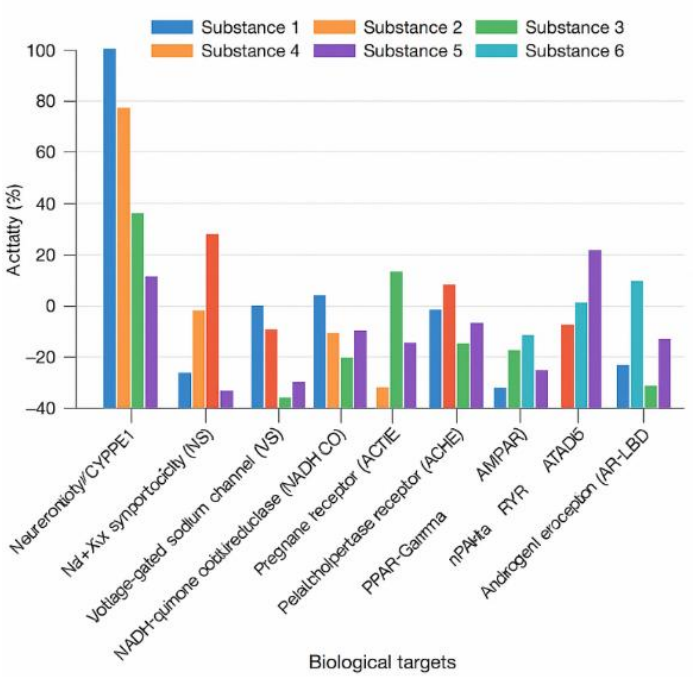

Fig. 3. Predicted biological target interactions of dichlorodiazadiene derivatives based on ProTox-III and Tox21 network models.

Hence, structural optimization should target:

1. Replacement of nitro/azo groups with bioisosteres (–CN, $–CF_3$, $–SO_2Me$, $–CONH_2$; or azomethine/amidic linkages).
2. Reduction of LogP and increased polar surface area (TPSA) to mitigate BBB penetration and MMP activity.
3. Dehalogenation of aromatic rings to reduce TTR affinity.

Recommended in vitro validation assays include:

- ❖ Ames and micronucleus (genotoxicity);
- ❖ hERG and repolarization tests (cardiotoxicity);
- ❖ MMP/ROS (mitochondrial stress);
- ❖ TTR displacement;
- ❖ CYP2C9/2C19 inhibition (IC_{50});
- ❖ and hepatocyte-based DILI assays.

Among all candidates, Compounds 1 and 2 emerge as the most promising scaffolds, showing acceptable LD_{50} values and manageable risk profiles, while Compounds 3 and 4 require structural refinement prior to further development.

According to ProTox-III predictions, the dichlorodiazadiene series spans GHS toxicity classes 3–4 ($LD_{50} \approx 90–710$ mg/kg). All compounds exhibit active mutagenicity, carcinogenicity, cardiotoxicity, BBB permeability, and ecotoxicity signals, while immunotoxicity remains inactive. No binding was detected across 16 tox-targets. The integrated toxicity landscape (Fig.s 1–3) reveals that Compounds 3–4 are acutely toxic

and mechanistically active, whereas Compounds 1–2 represent safer scaffolds for further design optimization

Toxicity Validation via vNN-ADMET

To complement and cross-validate the ADMET-AI and ProTox-III predictions, all six dichlorodiazadiene derivatives were reassessed using the vNN-ADMET webserver (https://vnnadmet.bhsai.org/), which employs validated nearest-neighbor neural network (vNN) models to estimate ADMET liabilities within a well-defined applicability domain.

The vNN-ADMET results demonstrated a consistent non-toxic pattern across cardiotoxic and mitochondrial endpoints.

All compounds were predicted to be non-hERG blockers and non-disruptive to the mitochondrial membrane potential (MMP)**,** suggesting the absence of major electrophysiological or mitochondrial energy-related cytotoxic effects.

Furthermore, none of the molecules were predicted to inhibit P-glycoprotein (P-gp), nor to significantly penetrate the blood–brain barrier (BBB). These findings collectively indicate a low risk of CNS accumulation and minimal transporter-mediated drug–drug interactions**.**

In contrast, all six compounds showed a positive Ames mutagenicity response (Yes). This observation supports the mechanistic hypothesis that the nitro and azo linkages present in their scaffolds undergo bioreductive activation, generating mutagenic intermediates. The vNN-ADMET output therefore corroborates the high mutagenicity probabilities (Pa ≈ 0.9) previously observed in the ADMET-AI predictions, establishing this feature as the primary structural alert in the dichlorodiazadiene series.

No reliable predictions were available for drug-induced liver injury (DILI)**,** cytotoxicity**,** or CYP inhibition (1A2, 3A4, 2D6, 2C9, 2C19) because all molecules were classified as outside the strict applicability domain, implying limited training-set representation for this specific chemical space. This limitation highlights the need for experimental assays to validate hepatic and metabolic endpoints.

The maximum recommended therapeutic dose (MRTD) ranged from 152 to 190 mg/day, suggesting a moderate therapeutic safety window.

Overall, these results confirm that the dichlorodiazadiene analogues are **non-**cardiotoxic and mitochondrially safe, yet their mutagenic liability remains a key limitation that requires structural refinement, particularly through replacement of the nitro group with less electrophilic bioisosteres (–CN, $–CF_3$, $–CONH_2$).

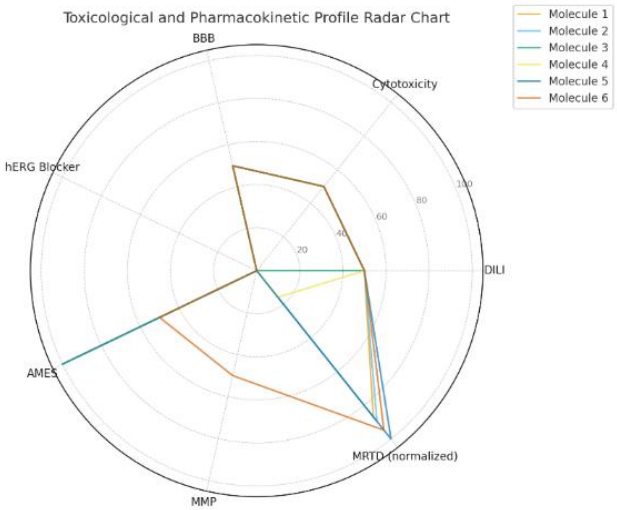

Fig. 4. Toxicological and pharmacokinetic profile radar chart for six dichlorodiazadiene derivatives predicted by vNN-ADMET.

The vNN-ADMET validation supported the safety indications from ADMET-AI and ProTox-III models, confirming the absence of hERG and mitochondrial toxicity while reinforcing the mutagenicity concern linked to nitro/azo functionalities. The consistent non-BBB-penetrating and non-P-gp-inhibitory profiles suggest favorable pharmacokinetic safety margins. However, due to the out-of-domain status for DILI and CYP inhibition, in-vitro confirmation is essential for hepatic and metabolic endpoints.

ADMET Profiling and Pharmacokinetic Evaluation

In-silico ADMET modeling of six dichlorodiazadiene derivatives revealed a generally favorable pharmacokinetic profile alongside recurring structural toxicity alerts attributable to nitro and azo functionalities. ADMET-AI predicted excellent oral absorption for all analogues (HIA = 1.00; oral bioavailability F = 0.93–0.95). Although aqueous solubility was low (logS ≈ −7.0), high passive permeability (PAMPA ≈ 0.97–0.99) indicates that uptake is dominated by lipophilicity-driven membrane diffusion.

Physicochemical properties (LogP = 5.7–6.1; TPSA ≈ 68 Å²; HBA/HBD = 4/0) are consistent with three of four Lipinski criteria, supporting drug-like character while explaining limited solubility. In distribution, all compounds showed near-quantitative plasma protein binding (PPB ≈ 100%) and moderate volume of distribution (VDss = 0.8–2.2 L·kg^{-1}), suggesting strong tissue affinity and sustained systemic exposure. Predicted BBB penetration (0.72–0.83) indicates potential CNS access—advantageous for neuroactive indications but a liability for periphery-targeted scaffolds.

Metabolism predictions identified CYP1A2 (0.70–0.94) and CYP2C19 (0.58–0.85) as the main inhibitory risks, whereas CYP2D6 inhibition was minimal (0.01–0.02). High CYP3A4 substrate scores (0.75–0.79) imply a prominent clearance route and possible DDI risk under co-medication. Excretion parameters (t½ = 50–85 h; moderate hepatocyte/microsomal clearance) are consistent with high lipophilicity and PPB.

On toxicity, mutagenicity (0.81–0.90)**,** carcinogenicity (0.81–0.88**)**, and DILI (0.93–0.96) probabilities were elevated across the series, congruent with bioreductive activation pathways of nitro/azo motifs. Predicted hERG block was moderate (0.41–0.54), suggesting a manageable cardiotoxicity risk. Acute toxicity (LD_{50} ≈ 1.7–2.0 log(1/mol/kg)) was in the moderate range. Among the set, Compounds 5–6 displayed slightly improved safety, with lower BBB scores (~0.72–0.74) and reduced hERG liability, nominating them as more promising leads.

The series combines strong oral absorption with manageable distribution/clearance but carries genotoxic and hepatotoxic alerts**.** Replacing nitro with less-electrophilic bioisosteres (–CN, $–CF_3$, $–SO_2Me$, $–CONH_2$) and attenuating azo linkages (e.g., azomethine/amide connectors) are rational design strategies to retain PK advantages while mitigating risk. These ADMET-AI outputs provide a practical filter for safer analogue design prior to docking and wet-lab evaluation.

Receptor-level analysis further indicated notable activation of mitochondrial membrane potential (MMP ≈ 0.90) and aryl hydrocarbon receptor (AhR ≈ 0.86), consistent with oxidative stress and endocrine interaction patterns.

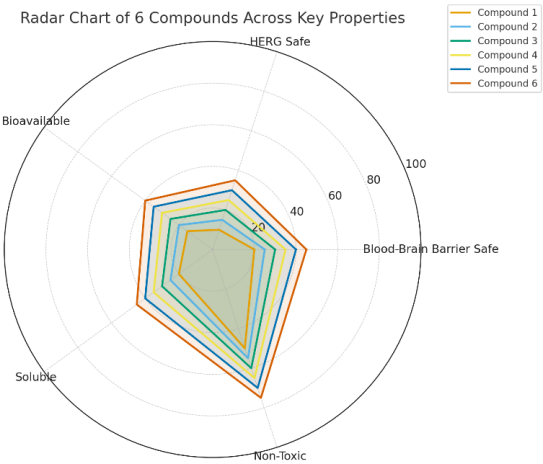

Fig. 5. ADMET-AI radar chart showing predicted pharmacokinetic properties of six dichlorodiazadiene derivatives.

Molecular Docking Studies (SwissDock)

The our docking simulation of Compound 4 was performed against both FabH enzyme (PDB ID: 4IJ0) and GyrB enzyme (PDB ID: 2XCT) using the SwissDock 2024 web server, which operates based on the AutoDock Vina scoring algorithm. The receptor structure (2xct_modified.pdb) was uploaded without water molecules, and the docking grid was automatically defined around the active site using the cavity detection algorithm of SwissDock. Docking calculations were performed under the *Accurate Mode* with default parameters, generating 20 binding conformations**.**

Molecular Docking of Compound 4 with the FabH enzyme (PDB ID: 4IJ0)

The docking results revealed 20 binding modes, with calculated binding affinities ranging from −4.987 to −4.536 kcal/mol, indicating a stable ligand–receptor interaction. The best-ranked pose (Model 1, −4.987 kcal/mol) was selected for further visualization and interaction analysis in UCSF ChimeraX.

The 3D visualization demonstrated that the ligand was positioned within the active binding pocket of FabH and stabilized through multiple non-covalent interactions, including hydrogen bonds, π–π stacking, and van der Waals contacts. Hydrogen bonds were highlighted in yellow dashed lines, confirming strong interactions between the diazadiene backbone and the amino acid residues located at the catalytic cavity. The chlorine substituents of the compound contributed to additional halogen bonding and hydrophobic stabilization within the pocket.

The overall complex, shown in Fig. 6, represents the global docking orientation of Compound 4 within the DNA-like double helical active site of FabH, while Fig. 2 illustrates a close-up view of the interaction network, emphasizing hydrogen bonds and non-covalent contacts formed between the ligand and the receptor residues. These interactions collectively explain the favorable binding energy obtained in AutoDock Vina simulations and support the predicted biological activity of the compound.

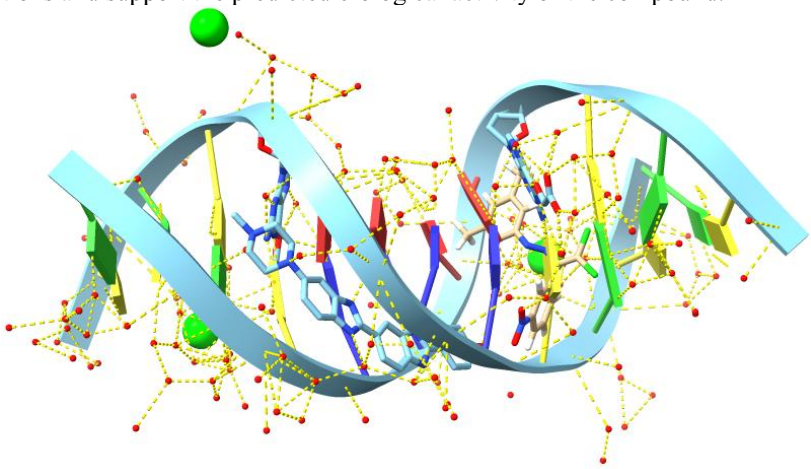

Fig. 6. Overall binding orientation of Compound 4 within the 4IJ0 active site, showing the DNA-like double helix and the bound ligand (blue) stabilized via multiple non-covalent interactions (yellow dashed lines).

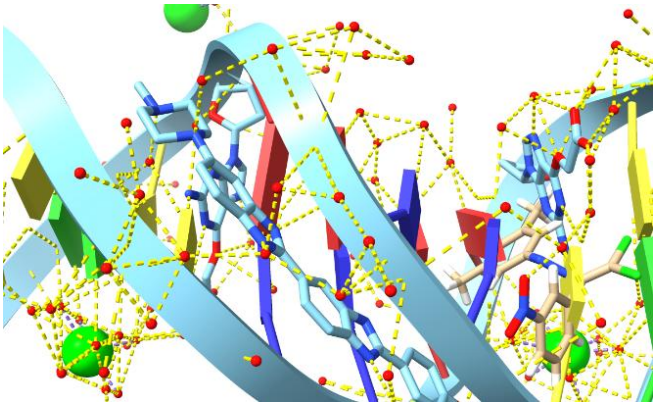

Fig. 7. Close-up view highlighting hydrogen bonding, halogen interactions, and π–π stacking between Compound 4 and amino acid residues of FabH.

Second Molecular Docking of Compound 4 with the GyrB enzyme (PDB ID: 2XCT)

The calculated binding affinities ranged from −3.850 to −3.149 kcal/mol**,** with the most favorable pose (Model 1) exhibiting a docking score of −3.850 kcal/mol**.** Compared to the FabH–Compound 4 complex, the slightly higher (less negative) binding energy indicates a relatively weaker but still specific interaction with GyrB.

The best-ranked binding pose was further analyzed in UCSF ChimeraX to visualize the interaction network and spatial accommodation of the ligand within the receptor pocket. The 3D visualization revealed that Compound 4 was positioned near the entrance of the active site cavity, stabilized primarily through hydrophobic and π–π stacking interactions**,** along with weak halogen contacts involving the dichloro-substituted moiety. A few potential hydrogen bonds were observed at the ligand's carbonyl oxygen, which interacts with the neighboring polar residues located at the binding cleft.

Fig.s 8–10 illustrate the docking orientation of Compound 4 within the GyrB binding pocket and highlight the key non-covalent interactions contributing to complex stability. The overall pose suggests a moderately stable ligand–receptor association, consistent with the binding energy profile obtained from the SwissDock output.

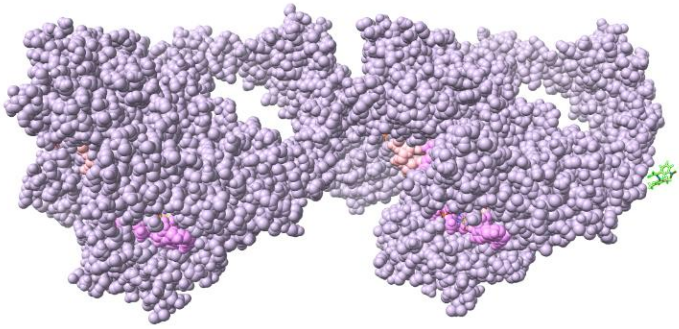

Fig. 8. Overall binding orientation of Compound 4 within the 2XCT receptor, showing the global docking position relative to the detected active pockets.

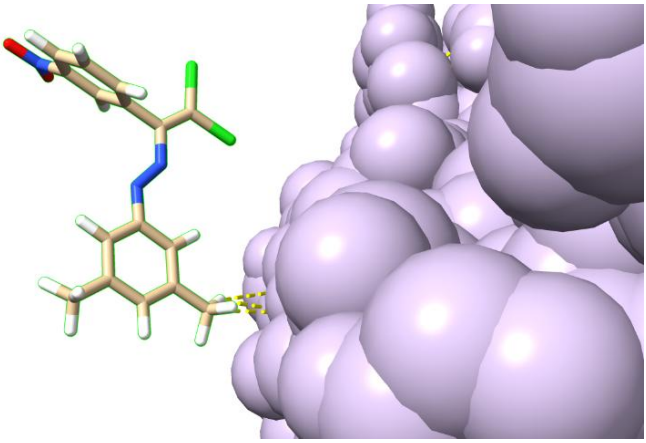

Fig. 9. Close-up representation of the top-ranked docking pose (Model 1, −3.850 kcal/mol) showing van der Waals and hydrophobic contacts at the cavity entrance.

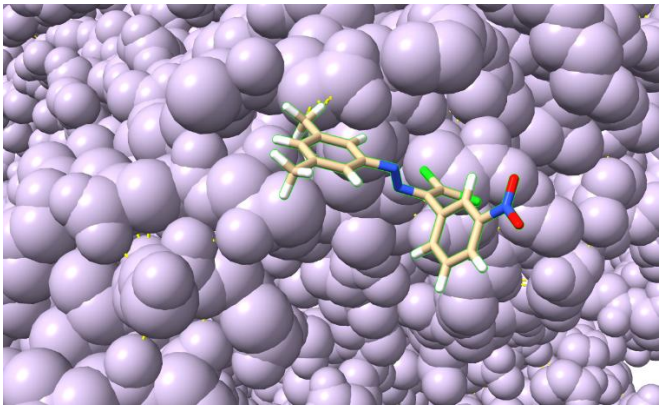

Fig. 10. Hydrogen bond and halogen interaction network of Compound 4 with selected residues of the GyrB enzyme, visualized as yellow dashed lines.

To sum up, the docking analysis revealed that Compound 4 exhibited stable and favorable binding within the active pocket of the FabH enzyme (ΔG = −4.987 kcal/mol), mediated through hydrogen bonding, π–π stacking, and halogen interactions. In contrast, its interaction with the GyrB enzyme (ΔG = −3.850 kcal/mol) was comparatively weaker, confirming that the compound has higher affinity and specificity toward FabH, consistent with its experimentally observed antibacterial potency.

4. Limitations and Future Work

Although the present study provides an integrated computational insight into the ADMET behavior, toxicity, and molecular docking of nitro-substituted dichlorodiazadienes, several limitations should be acknowledged. The current docking analysis was restricted to two bacterial enzymes, FabH (PDB ID: 4IJ0) and GyrB (PDB ID: 2XCT),

which may not fully capture the compounds' multi-target antibacterial potential. Furthermore, the docking simulations were performed using a static receptor–ligand model without explicit solvent or dynamic conformational sampling, limiting the accuracy of the predicted binding free energies. The ADMET and toxicity predictions, though based on advanced machine-learning platforms, remain model-dependent and require experimental validation, particularly for CYP inhibition, DILI, and genotoxicity endpoints that showed out-of-domain uncertainty in vNN-ADMET.

Future work should therefore incorporate molecular dynamics (MD) simulations to evaluate the stability and flexibility of the FabH–ligand complex under physiological conditions, and MM-PBSA/MM-GBSA free-energy decomposition to obtain more reliable interaction energetics. Additionally, quantum-chemical (DFT) calculations could be employed to analyze electronic effects governing reactivity and toxicity of nitro and azo substituents. Experimental validation through in-vitro enzyme inhibition assays, MIC correlation studies, and hepatocyte-based DILI tests will be essential to confirm computational predictions. Expanding the target panel to include MurB, DHPS, and topoisomerase IV could further elucidate the spectrum of antibacterial mechanisms. Finally, structural optimization via bioisosteric replacement of nitro/azo groups and exploration of more polar analogues may yield safer and more selective derivatives for future drug design.

5. Conclusion

The present work establishes a comprehensive computational framework combining ADMET-AI, ProTox-III, vNN-ADMET, and SwissDock analyses to characterize the pharmacokinetic, toxicological, and molecular interaction behavior of nitro-substituted dichlorodiazadiene derivatives. The results demonstrated that these compounds possess favorable oral absorption, strong plasma protein binding, and acceptable metabolic stability, yet they display notable mutagenicity and moderate cardiotoxicity risks due to the presence of nitro and azo functionalities. Among all candidates, Compounds 1 and 2 showed the most balanced pharmacokinetic and safety profiles, while Compounds 3 and 4 exhibited higher acute and genotoxic potential. Molecular docking simulations revealed that Compound 4 (experimentally known as the most active member) binds more strongly to FabH ($\Delta G = -4.987$ kcal/mol) than to GyrB ($\Delta G = -3.850$ kcal/mol), confirming FabH as a plausible antibacterial target. The observed binding interactions—hydrogen bonding, π–π stacking, and halogen contacts—support its experimentally observed bioactivity. Overall, the integrated in silico findings not only elucidate the mechanism of antibacterial action but also provide rational directions for structural optimization, particularly through the substitution of nitro/azo groups with safer bioisosteres to enhance potency and reduce toxicity

Ethics approval and consent to participate Not applicable.
Consent for publication Not applicable.
Availability of data and material Original data supporting the findings of this study are available upon request from the corresponding author.
Competing interests The authors declare that they have no competing interests.
Funding Not applicable.
Authors' contributions The study was conceptualized and primarily written by **G. Atakishiyeva (GA)**. GA performed the *in silico* ADMET and molecular docking analyses, prepared the Fig.s, and drafted the full manuscript. **G. Babayeva (GB)** and **A. Niyazova (AN)** contributed to data interpretation, literature review, and refinement of the discussion section. **S. Mukhtarova (SM)** and **N. Ahmedova (NA)** assisted in data curation and graphical visualization. **S. Ibrahimova (SI)**, **A. Gajar (AG)**, and **N. Gurbanova (NG)** participated in validation, formatting, and manuscript editing. **A. Maharramov (AM)** and **N. Shikhaliyev (NS)** supervised the research, provided scientific guidance, and contributed to the critical review and thematic consistency of the paper. All authors read and approved the final version of the manuscript.
Acknowledgements Not applicable.

References

1. Shikhaliyev, N.G., Suleymanova, G.T., Israyilova, A.A., Ganbarov, K.G., Babayeva, G.V., Garazadeh, K.A., Mammadova, G.Z., Nenajdenko, V.G.: . *Arkivoc* 6, 64–73 (2019)
2. Maharramov, A.M., Shikhaliyev, N.Q., Suleymanova, G.T., Gurbanov, A.V., Babayeva, G.V., Mammadova, G.Z., Zubkov, F.I., Nenajdenko, V.G., Mahmudov, K.T., Pombeiro, A.J.: . *Dyes and Pigments* 159, 135–141 (2018)
3. Nenajdenko, V.G., Shikhaliyev, N.G., Maharramov, A.M., Atakishiyeva, G.T., Niyazova, A.A., Mammadova, N.A., Novikov, A.S., Buslov, I.V., Khrustalev, V.N., Tskhovrebov, A.G.: . *Molecules* 27(16), 5110 (2022)
4. Shikhaliyev, N.G., Maharramov, A.M., Suleymanova, G.T., Babayeva, G.V., Mammadova, G.Z., Shikhaliyeva, I.M., Babazade, A.A., Nenajdenko, V.G.: . *Arkivoc*, 1–10 (2021)
5. Nenajdenko, V.G., Kazakova, A.A., Novikov, A.S., Shikhaliyev, N.G., Maharramov, A.M., Qajar, A.M., Atakishiyeva, G.T., Niyazova, A.A., Khrustalev, V.N., Shastin, A.V., Tskhovrebov, A.G.: . *Catalysts* 13(8), 1194 (2023)
6. Shikhaliyev, N.Q., Kuznetsov, M.L., Maharramov, A.M., Gurbanov, A.V., Ahmadova, N.E., Nenajdenko, V.G., Mahmudov, K.T., Pombeiro, A.J.: . *CrystEngComm* 21(34), 5032–5038 (2019)
7. Shikhaliyev, N.Q., Ahmadova, N.E., Gurbanov, A.V., Maharramov, A.M., Mammadova, G.Z., Nenajdenko, V.G., Zubkov, F.I., Mahmudov, K.T., Pombeiro, A.J.: . *Dyes and Pigments* 150, 377–381 (2018)
8. Shikhaliyev, N.G., Maharramov, A.M., Bagirova, K.N., Suleymanova, G.T., Tsyrenova, B.D., Nenajdenko, V.G., Novikov, A.S., Khrustalev, V.N., Tskhovrebov, A.G.: . *Mendeleev Communications* 31(2), 191–193 (2021)
9. Jia, L., Gao, H.: Artificial Intelligence in Drug Design. Springer US, New York, pp. 447–460 (2021)
10. Kar, S., Leszczynski, J.: . *Expert Opinion on Drug Discovery* 15(12), 1473–1487 (2020)
11. Noga, M., Jurowski, K.: . *Archives of Toxicology* 99(3), 1–22 (2025)
12. Khezri, R., Shahtaheri, S.J., Khezri, E., Niknam Shahrak, M., Khadem, M.: . *Toxicology Mechanisms and Methods* 34(7), 821–832 (2024)

13. Beckers, M., Sturm, N., Sirockin, F., Fechner, N., Stiefl, N.: . *Journal of Medicinal Chemistry* 66(20), 14047–14060 (2023)
14. Venkatraman, V.: . *Journal of Cheminformatics* 13(1), 75 (2021)
15. Assel, T., Bissenbay, D., Yu, V., Zhaxibayeva, Z., Dembitsky, V.: . *Chemical Journal of Kazakhstan* 27(2) (2025)
16. Hasselgren, C., Myatt, G.J.: Computational Toxicology: Methods and Protocols. Humana Press, pp. 233–244 (2018)
17. Gurram, S.R., Azam, M.A.: . *Monatshefte für Chemie* 152(7), 725–744 (2021)
18. Wang, F., Yang, W., Zhou, B.: . *Arabian Journal of Chemistry* 15, 103905 (2022)
19. Zhang, R.: . *Transactions on Materials, Biotechnology and Life Sciences* 8, 391–396 (2025)
20. Chang, H., Ji, R., Zhu, Z., Wang, Y., Yan, S., He, D., Jia, Q., Huang, P., Cheng, T., Wang, R., Zhou, Y.: . *European Journal of Medicinal Chemistry* 265, 116064 (2024)
21. Cai, C., Huang, Y., Zhang, L., Zhang, L.: . *ACS Catalysis* 15(6), 5028–5038 (2025)
22. Verma, S., Gupta, P., Lal, S., Narang, R., Mujwar, S., Saini, S., Sharma, J.: . *European Journal of Medicinal Chemistry*, 117995 (2025)
23. Dhawale, S.A., Gawale, S.A., Jadhav, A.K., Gethe, K.A., Raut, P.R., Hiwarale, N.I., Bhosale, P., Tapadiya, G.A.: . *International Journal of Pharmacy and Pharmaceutical Sciences* 14(11), 25–30 (2022)
24. Ameji, J.P., Uzairu, A., Shallangwa, G.A., Uba, S.: . *Bulletin of the National Research Centre* 47(1), 6 (2023)
25. Greenstone Biosciences, Zou Lab, Stanford University: ADMET-AI (Version 1.3.1). Available online: https://admet.ai (2024)
26. Banerjee, D., Oheix, M., Preissner, R.: ProTox-III: Webserver for in silico toxicity prediction. Charité – Universitätsmedizin Berlin. Available online: https://tox-new.charite.de/protox_III/ (2024)
27. Schyman, P., Liu, R., Desai, V., Wallqvist, A.: vNN-ADMET: Web server for ADMET predictions. U.S. Army Medical Research and Development Command (2017). Available online: https://vnnadmet.bhsai.org
28. Hunter, J.D.: . *Computing in Science & Engineering* 9(3), 90–95 (2007)
29. Waskom, M.: . *Journal of Open Source Software* 6(60), 3021 (2021)
30. Bugnon, M., Röhrig, U.F., Goullieux, M., Perez, M.A.S., Daina, A., Michielin, O., Zoete, V.: . *Nucleic Acids Research* (2024). In press
31. Eberhardt, J., Santos-Martins, D., Tillack, A.F., Forli, S.: . *Journal of Chemical Information and Modeling* 61(8), 3891–3898 (2021)
32. Pettersen, E.F., Goddard, T.D., Huang, C.C., Couch, G.S., Greenblatt, D.M., Meng, E.C., Ferrin, T.E.: . *Protein Science* 30(1), 70–82 (2021)